

Atoms in parallel fields: Analysis with diffractive periodic orbits

S. M. Owen, T. S. Monteiro, and P. A. Dando*

Department of Physics and Astronomy, University College London, Gower Street, London, WC1E 6BT, United Kingdom

(Received 25 February 2000)

We show that fluctuations in the density of states of nonhydrogenic atoms in parallel fields are strongly influenced by diffractive periodic orbits. Unlike typical systems with a diffractive point scatterer, the atomic core of small atoms like lithium and helium is best understood as a combined geometric and diffractive scatterer. Each Gutzwiller (geometric) periodic orbit is paired with a diffractive orbit of the same action. We investigate, particularly, amplitudes for contributions from repetitions, and multiple scattering orbits. We find that periodic orbit repetitions are described by ‘‘hybrid’’ orbits, combining both diffractive and geometric core scatters, and that by including all possible permutations we can obtain excellent agreement between the semiclassical model and accurate fully quantal calculations. For high repetitions, we find even one-scatter diffractive contributions become of the same order as those of the geometric periodic orbit for repetition numbers $n \sim \hbar^{-1/2}$. Although the contribution of individual diffractive orbits is suppressed by $O(\hbar^{1/2})$ relative to the geometric periodic orbits, the proliferation of diffractive orbits with increasing period means that the diffractive effect for the atom can persist in the $\hbar \rightarrow 0$ limit.

PACS number(s): 05.45.-a, 03.65.Sq, 32.60.+i

I. INTRODUCTION

Highly excited (Rydberg) atoms in the presence of static external magnetic and/or electric fields provide some of the best examples of experimental studies of the effects of chaos and classical orbits [1]. A very useful feature of these systems is their scaling property: the classical motion does not depend on the electron energy and the magnetic and electric field strengths separately, but only on a single parameter: the *scaled* energy. In the case of diamagnetic hydrogen, the classical motion undergoes a gradual transition from regularity to full chaos as this parameter is varied. With the development of experimental fixed scaled-energy spectroscopy [2], and methods for calculating fully quantal spectra at a constant scaled energy, it has been possible to make detailed comparisons between the quantum and classical dynamics of both diamagnetic hydrogen [3,4] and nonhydrogenic [5,6] atoms. In particular, frequencies and amplitudes of long-range modulations in the density of states of highly excited hydrogen atoms in a static magnetic field have been described quantitatively using periodic orbit (PO) theory [7] in the form of the well-known Gutzwiller trace formula (GTF) [8].

The spectra of nonhydrogenic atoms in weak fields, however, were found to have unexpected properties not seen in hydrogen. Comparisons between accurate quantum spectra revealed spectral amplitudes for nonhydrogenic atoms that differed substantially from those of hydrogen [5]. In addition, experimental measurements of diamagnetic helium atoms found modulations, not seen in hydrogen, which were identified as resulting from combinations of hydrogenic periodic orbits that arise from scattering with the nonhydrogenic core [6]. Similar structures were found in the experimental Stark (pure electric field) spectrum of lithium [9].

More recently, the spectra of nonhydrogenic atoms in weak fields were shown to be associated with a new generic class of intermediate energy level statistics. Nearest-neighbor spacing (NNS) distributions were found [10,11] to be neither Poissonian (regular) nor Wigner-Dyson (chaotic), but close to a distribution [$P(s) = 4se^{-2s}$] called a *semi-Poisson* distribution. Such intermediate spectra are also of broad current interest in mesoscopic systems [12–15].

These observations have led, in recent years, to much interest in the phenomenon of so-called *core-induced chaos* [5,6,9,16–19] in the dynamics of Rydberg atoms in external fields. The unexpected features in the nonhydrogenic spectra were variously interpreted as arising from chaos due to the effect of the inner multi-electron core [9,18] or as \hbar -dependent corrections [19] which were semiclassically vanishing.

It was since shown [20] that modulations of the eigenvalue spectra of nonhydrogenic atoms in weak fields due to periodic orbits can be described semiclassically at a quantitative level *only* if diffractive corrections are included. In addition, a semiclassical analysis of spectral rigidities for atoms in electric fields (integrable with diffraction) revealed that there are substantial core-induced effects due to diffractive one-scatter orbits which do not vanish in the semiclassical limit [21]. Another recent semiclassical study of general *chaotic* systems with diffraction considered scattering to all orders [22]. For chaotic dynamics, the number of ordinary (geometric) PO's proliferates exponentially with increasing period T . However, it was shown [22] that the number of diffractive orbits in a generic chaotic system with diffraction grows even more rapidly. Indeed, the number of one-scatter trajectories increases faster than the number of geometric PO's by a factor of T .

Diffraction in atoms (Coulomb plus short range scatterer) differs in key respects from typical diffractive billiards. The additional presence of the Coulomb term means that every diffractive orbit is paired with a geometric periodic orbit or half-periodic orbit, even in the chaotic regime. In contrast,

*Present address: Department of Chemistry, University of Southern California, Los Angeles, CA 90089-0482.

for billiard problems, diffractive and isolated geometric PO's are unrelated [22–24]. The diffractive effect in chaotic atoms is expected to differ significantly from that in billiard problems.

Atomic spectral properties and statistics depend strongly on the interference between groups of contributions of the same action, but with different phases and amplitudes. Adding these correctly is nontrivial. For example, the dominant effect in long-range statistics was found to be due to the “off-diagonal” contributions between geometric POs and diffractive one-scatter orbits of the same action [21]. In semiclassical studies of atomic photoabsorption (closed orbit theory) [25–28,19] an analogous effect—the gradual suppression of the amplitude of high harmonics by core-scattering terms of the same action—was termed “core shadowing.” Experimental photoabsorption spectra, however, probe closed, rather than periodic, orbits. In a previous paper [20] we proposed a model which combined standard PO theory with diffractive corrections for a few short primitive periodic orbits in diamagnetic atoms. This was the first successful application of periodic orbit theory, in the form of the GTF, to nonhydrogenic Rydberg atoms. One of the main results shown in Ref. [20] is that, in periodic orbit theory with core-scattering, core shadowing affects even primitive orbits.

In this paper we investigate in particular multiple scatterings, and give a prescription for obtaining the correct multiplicities for different types of diffractive orbits. The motivation for this work is, broadly, to establish a scheme for counting correctly, to all orders, atomic diffractive orbit contributions so as to further understanding of the persistence of these diffractive effects in the semiclassical limit. In particular, we investigate up to third order the core-shadowing terms, which are unique to the atomic systems. Since we found in Ref. [20] that some properties (such as phases and multiplicities of the important quasi-Landau orbit) were symmetry dependent, we test the model on atoms in parallel fields, which have different symmetry properties from the diamagnetic atom.

In Sec. II, we briefly review the calculations at a fixed scaled energy for both the classical and quantal cases. In Sec. III, we present details of the semiclassical calculation of diffractive amplitudes. The contribution of the diffractive orbits to the amplitude of first traversals of geometric PO's is studied in Sec. IV. In Sec. V we discuss the phases and multiplicities of different types of diffractive orbit. We explain the core shadowing in detail up to third order of one particular PO. In Sec. VI we present comparisons between our semiclassical and quantal results for core shadowing and other trajectories.

II. ATOMS IN PARALLEL FIELDS: SCALED SPECTRA

The scaling properties of the classical dynamics of Rydberg atoms in static magnetic fields were extensively reviewed elsewhere [4], so only a brief outline is given here. The classical dynamics of a hydrogen atom in a pure magnetic field (of strength B) depends only on a scaled energy $\varepsilon_B = EB^{-2/3}$. In a pure electric field (of strength F), the corresponding parameter is $\varepsilon_F = EF^{-1/2}$. It should be noted that the hydrogenic scaling property does not hold strictly in the

core region of nonhydrogenic atoms. However, it is appropriate to apply the same scaling transformation to nonhydrogenic atoms because the core region is very small when compared to the size of the highly excited Rydberg states.

The procedure for scaling the parallel field case is similar. The parallel field Hamiltonian [in cylindrical coordinates (ρ, z, ϕ) and atomic units with $m=0$] is

$$H = \frac{1}{2}(P_\rho^2 + P_z^2) - \frac{1}{r} + \frac{1}{8}B^2\rho^2 + Fz, \quad (1)$$

with $r = \sqrt{\rho^2 + z^2}$. Equation (1) can be rescaled by transforming position, momentum and time variables according to $r \rightarrow rB^{-2/3}$, $P \rightarrow PB^{1/3}$ and $t \rightarrow t/B$. Regularization, to remove the Coulomb singularity, is achieved by the usual procedure of transformation to semiparabolic coordinates $(\mu, \nu = \sqrt{r \pm z})$ and a rescaled time $d\tau = (\mu^2 + \nu^2)dt$, with conjugate momenta $P_\mu = d\mu/d\tau$ and $P_\nu = d\nu/d\tau$. The regularized, scaled Hamiltonian for hydrogen in parallel electric and magnetic fields now depends only on two parameters ε_F and ε_B , which completely determine the classical behavior, and is written as

$$\mathcal{H} = \frac{1}{2}(P_\mu^2 + P_\nu^2) - \varepsilon_B(\mu^2 + \nu^2) + V_{\text{ext}}(\mu, \nu) \equiv 2, \quad (2)$$

where

$$V_{\text{ext}} = \frac{1}{8}\nu^2\mu^2(\mu^2 + \nu^2) + \frac{1}{2}\left(\frac{\varepsilon_B}{\varepsilon_F}\right)^2(\mu^4 - \nu^4) \quad (3)$$

is the contribution from the external fields.

The equations of motion arising from the classical Hamiltonian of Eq. (2) were solved numerically to obtain the relevant classical trajectories, their actions, stability parameters, and Maslov indices.

When considering the classical dynamics of a nonhydrogenic atom in an external field, one possible approach [17,18] is to add a short-range “model” potential, which describes the non-Coulombic nature of the ionic core, to the Hamiltonian of Eq. (1). However, we do not use this approach here. Instead, we follow Ref. [20], and treat the system as hydrogenic with the multielectron core playing the role of a point diffractive source, as described in Sec. III below. With this prescription, the required periodic orbits are then those of the hydrogenic system described by Eq. (2).

For parallel fields, the corresponding scaled-coordinate Schrödinger equation (with $m=0$) takes the form

$$\left\{ -1/r + \frac{1}{8}\rho^2 + \left(\frac{\varepsilon_B}{\varepsilon_F}\right)^2 z - \varepsilon_B \right\} \psi_i = \frac{B_i^{2/3}}{2} \nabla^2 \psi_i. \quad (4)$$

The scaled energies ε_B and ε_F fix the classical behavior of the system. However, the dependence on the field (through the eigenvalue $B_i^{2/3}$) cannot be eliminated in the quantum case. Each $B_i^{2/3}$ eigenvalue corresponds to energy eigenvalues $E_i = \varepsilon_B B_i^{2/3}$. The set of eigenvalues $B_i^{2/3}$ all correspond to the same classical regime but as $B_i \rightarrow 0$ the quantum spectrum becomes increasingly dense: the square root of the eigenvalue plays the role of an effective Planck's constant, i.e., $B^{1/3} = \hbar_{\text{eff}}$. This can be seen by considering the momentum-

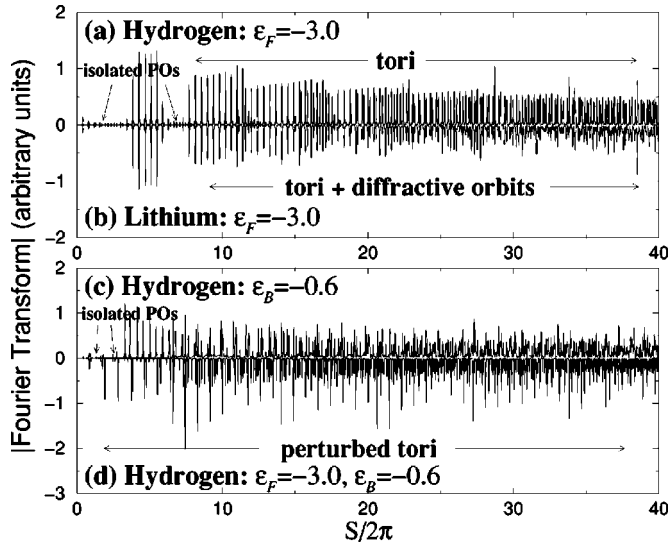


FIG. 1. Illustration of the different types of trajectories contributing to the density of states. (a) Fourier transformed spectrum of hydrogen in an electric field. For low action there are mainly weak contributions from isolated Gutzwiller PO's. For higher action there are mainly integrable tori, described by the Berry-Tabor formula [30]. (b) Fourier transformed spectrum of a lithiumlike atom in an electric field. There are now additional contributions from diffractive PO's. Their numbers proliferate rapidly for higher actions. (c) Fourier transformed spectrum of hydrogen in a magnetic field. (d) Fourier transformed spectrum of hydrogen in a parallel field. In both (c) and (d), the high action region is dominated by remnants of integrable tori. In this regime the Gutzwiller formula is not valid.

position commutator in scaled variables (atomic units are used throughout, hence $\hbar = 1$):

$$[pB^{-1/3}, qB^{2/3}] = iB^{1/3} = i\hbar_{\text{eff}}. \quad (5)$$

Fixed scaled-energy quantum spectra can be compared directly with semiclassical calculations. A Fourier transform with respect to \hbar_{eff}^{-1} yields sharp peaks at the *scaled* actions of classical orbits. The scaled action is simply related to the true action: $S(\varepsilon_F, \varepsilon_B) = B^{-1/3}S(E, F, B)$. The heights of these peaks yield accurate estimates of the semiclassical amplitudes.

In the case of nonhydrogenic atoms in external fields, most theoretical quantum solutions (see, e.g., Refs. [5,6]) follow a suggestion of Clark and Taylor [29] who noted that the problem splits conveniently into two regions: an outer region where the core is negligible, and an inner region where the external field can be neglected. In the inner region, the interaction of the outer electron with the ionic core can be accounted for by a set of angular momentum dependent phase shifts—the quantum defects—in each partial wave [33]. Separate solutions are obtained for the two regions and the wave functions matched at a boundary using an *R*-matrix type approach, yielding the required energy eigenvalues for the entire system. In the quantum calculations presented here, we have used a variant of this method where the *R*-matrix matching procedure is replaced by the inclusion of a Schneider term on the boundary [6] to obtain levels 16 000–32 000 above the ground state.

In the pure magnetic field case both the azimuthal quantum number m and the z parity are good quantum numbers. In the parallel field case, only m is a good quantum number, since the parallel field breaks the symmetry about $z=0$, destroying parity conservation. All calculations presented here are for $m=0$, $\varepsilon_B = -0.6$, and $\varepsilon_F = -3.0$. The classical dynamics for a hydrogen atom in a pure magnetic field with $\varepsilon_B = -0.6$ is near integrable. The pure electric field (Stark spectra) is integrable for all ε_F , and its NNS statistics are Poissonian: $P(s) = e^{-s}$. In both cases, the nonhydrogenic NNS statistics are intermediate, $P(s) = \alpha s e^{-\alpha s/2}$, with the diamagnetic atom close to half-Poisson, with $\alpha \approx 4$.

Differences between the spectra of hydrogen and nonhydrogenic atoms in pure magnetic, electric, and parallel fields are summarized in Fig. 1. The magnitude of the Fourier transform of the quantum mechanically calculated spectrum of hydrogen in a static electric field at $\varepsilon_F = -3.0$ is shown in Fig. 1(a). At low scaled actions, $0 \leq S/(2\pi) \leq 7$, there are a number of weak contributions arising from isolated Gutzwiller PO's. At higher actions, the main peaks arise from contributions of tori, and are well described by the Berry-Tabor formula [30] for integrable systems. Figure 1(b) shows the corresponding Fourier transformed spectrum of a lithiumlike atom in an electric field. At low scaled actions there are again weak contributions from the isolated periodic orbits. At higher scaled actions, significant differences from that of the hydrogenic case can be seen. Here, in addition to the torus effects, are contributions arising from diffractive orbits which occur due to the presence of the ionic core. The number of such diffractive orbits proliferates rapidly at higher scaled actions.

Figure 1(c) shows the Fourier transformed spectrum of hydrogen in a static magnetic field at $\varepsilon_B = -0.6$. The classical dynamics of the diamagnetic hydrogen atom is nonintegrable. However, it remains near-integrable for $\varepsilon_B = -0.6$ and, in the high scaled-action regime, the spectrum is dominated by contributions from perturbed tori. The situation is similar for hydrogen in parallel fields with $\varepsilon_F = -3.0$ and $\varepsilon_B = -0.6$, which is shown in Fig. 1(d). Here contributions from tori, evident at large scaled actions in the pure electric field case shown in Fig. 1(a), are modified by the presence of the weak magnetic field; the spectrum is dominated in this region by contributions from the remnants of integrable tori. Only those orbits, with a reasonably low scaled action, may be considered isolated and amenable to treatment with the GTF. Semiclassical trace formulas for the density of states of near-integrable systems have been derived [31], but we will not use these here. Instead, we restrict our detailed comparisons between semiclassical and quantal spectra of nonhydrogenic atoms in parallel fields to the region $0 \leq S/(2\pi) \leq 5$.

Theoretical and experimental investigations of atomic photoabsorption in parallel fields at a constant scaled energy have been undertaken previously in Ref. [32]. But only in Ref. [20] was the Gutzwiller formula applied for the first time to a generic diamagnetic atom. Hence to our knowledge this represents the first semiclassical analysis of the density of states (as opposed to photoabsorption spectra) for atoms in *parallel* fields.

III. SEMICLASSICAL CALCULATIONS: GEOMETRIC AND DIFFRACTIVE PERIODIC ORBITS

An important approach to the quantization of nonintegrable, time independent Hamiltonian systems is via periodic

orbit theory (POT) in the form of the well-known GTF. In standard POT, the density of states (DOS), $\rho(E) = \sum_i \delta(E - E_i)$, is calculated from the trace of the semiclassical Green's function: $\rho(E) = -(1/\pi) \text{Im Tr } G_{\text{SC}}$. The trace can be decomposed into a sum of smooth and oscillating components: $\rho(E) = \rho_{\text{sm}}(E) + \rho_{\text{osc}}(E)$. The oscillations in $\rho_{\text{osc}}(E)$ are given quantitatively by the GTF as a sum of contributions from the isolated POs.

In diffractive periodic orbit theory (DPOT) [23], the Green's function is expressed as the sum of a geometric and a diffractive component:

$$\rho(E) = -\frac{1}{\pi} \text{Im Tr } G_g(E) - \frac{1}{\pi} \text{Im Tr } G_D(E). \quad (6)$$

Correspondingly, oscillations in the density of states $\rho(E)$ now have one contribution from geometric PO's and another from diffractive orbits.

The GTF yields a good description of the amplitudes of the geometric component. The diffractive component arises from trajectories which meet a discontinuity in the potential or a dynamical structure comparable in size to the de Broglie wavelength. This could be, for example, the sharp vertex in a cardioid billiard. A ray incident at a vertex at point x_0 produces an outgoing source α_{diff} which is proportional to the semiclassical Green's function at the incidence of the ray, i.e., $\alpha_{\text{diff}} = d(\theta, \theta') G_{\text{SC}}(x, x_0)$ [23]. The diffraction constant $d(\theta, \theta')$ quantifies the angular redistribution of the amplitude of an incident ray due to the diffraction. An orbit with a single scatter at the diffractive point x_0 contributes a term $\alpha_{\text{diff}}(x, x_0) G_{\text{SC}}(x_0, x')$ to $G_D(x, x')$. A key result proven in Ref. [23] is that the trace of G_D is simply proportional to $dG_{\text{SC}}(x_0, x_0)$. In particular, the contribution of the k th single-scatter diffractive trajectory to the trace of G_D is

$$A_k \exp\{i(S_k + \Phi_k)\} = \frac{T_k}{i\hbar} d(\theta_k, \theta'_k) G_{\text{SC}}^k(x_0, x_0), \quad (7)$$

where G_{SC}^k is the contribution to the semiclassical Green's function along classical trajectory k starting and returning to the diffractive point x_0 , A_k is an amplitude, S_k is the classical action, and Φ_k includes other phases such as the Maslov index. For multiple scatters [23], it has been shown that, in general, the trace is obtained by taking products over contributions. Then,

$$\text{Tr } G_D = \sum_p \frac{T_p}{i\hbar} \prod_n d(n) G_{\text{SC}}(x_n, x_{n+1}), \quad (8)$$

where T_p is the total sum of (primitive) periods taken over the paths between the n th and $(n+1)$ th vertices.

We note that the expressions weighted by T_p refer to unscaled spectra. For scaled spectra, we require $\rho(B^{-1/3})$. Fortunately the well-known transformation to a scaled DOS is straightforward, and involves a simple change in the weighting factor; instead of T_p , we weight by the *scaled* action \tilde{S}_p . Hence, the scaled version of Eq. (7) (with $\hbar = 1$) is

$$\tilde{A}_k \exp\{i(B^{-1/3}\tilde{S}_k + \Phi_k)\} = \frac{\tilde{T}_k}{i} d(\theta_k, \theta'_k) \tilde{G}_D(x_0, x_0), \quad (9)$$

where the tilde refers to scaled quantities. For convenience, we drop the tildes below, but understand that all quantities refer to scaled calculations.

In Ref. [20], a prescription for adapting DPOT for the atomic case was presented. The atomic core gives rise to both Coulomb as well as short-range scattering. The latter is well described by quantum defect theory [33] parametrized by a set of quantum defects δ_l in each partial wave. For many atoms only the lowest partial waves have nonzero quantum defects. For example, for lithium $\delta_0 \approx 0.4\pi$ and $\delta_{l \geq 2} \approx 0$, while for triplet helium $\delta_0 \approx 0.3\pi$ and $\delta_{l \geq 2} \approx 0$.

The Coulomb part results in geometric orbits, described by the GTF. Hence there is a geometric component to which all periodic orbits make a contribution, regardless of whether they pass through the nucleus, and an additional diffractive part to which only orbits passing through the nucleus contribute.

A key difference with the standard DPOT approach results from the presence of the multielectron core and Coulomb divergence. We cannot write a (radial) semiclassical Green's function which is valid right up to the nucleus at $r = 0$. Instead, the problem of atomic core scattering is solved by matching quantal solutions using Coulomb waves and semiclassical waves on a *surface* $r = r_0$, outside the multielectron core. The formalism was originally developed to obtain closed orbit modulations of photoabsorption spectra [25,28], including combination recurrences [19].

However, we have found that we can, by analogy, obtain a similar expression to treat the DOS using Gutzwiller PO's with diffraction to a nonhydrogenic atom. We have an "external" form of the Green's function $G_{\text{SC}}(r_0, \theta, r_0, \theta')$ which propagates outgoing waves outward semiclassically from the surface $r = r_0$, and back again. We also need an internal, diffractive term $\alpha_{\text{diff}}(r_0, \theta, r_0, \theta')$ which relates an incoming ray incident on the core to an outgoing diffracted wave. The matching radius r_0 is arbitrary, subject to the constraint that it must lie outside the core, but within the region where a solution using Coulomb waves is valid (i.e., where the external field is negligible). Then we will have a contribution for a complete closed diffractive orbit of the form

$$\mathcal{G}(\theta, \theta') = \alpha_{\text{diff}}(r_0, \theta, r_0, \theta') G_{\text{SC}}(r_0, \theta, r_0, \theta'). \quad (10)$$

The amplitude cannot depend on the matching radius, so an obvious requirement is that $\mathcal{G}(\theta, \theta')$ should be independent of r_0 .

In a region near the core where the Coulomb interaction is dominant and the external field is negligible, the quantum wave function can be written as the sum of outgoing and incoming waves [25,28]:

$$\Psi = \psi_j^{\text{inc}} + \psi_{\text{scatt}}. \quad (11)$$

The incoming wave is a Coulomb wave, $\psi_j^{\text{inc}} = \psi_{\text{Coul}}^{(-)}$, which approaches the atomic core from infinity at an angle, θ_f^j , to the positive z axis. On reaching the core, $\psi_{\text{Coul}}^{(-)}$ produces a scattered wave ψ_{scatt} , which feeds outgoing semiclassical waves along periodic orbits, starting at any angle θ ; ψ_{scatt} can be decomposed further into an outgoing Coulomb wave together with a core-scattered wave [28]:

$$\psi_{\text{scatt}}(r, \theta) = \psi_{\text{Coul}}^{(+)}(r, \theta) + \psi_{\text{core}}^{\theta_f}(r, \theta). \quad (12)$$

The Coulomb part of the scattered wave is strongly back-focused along $\theta \approx \theta_f$, and can be written in closed form [28]. We equate $\psi_{\text{Coul}}^{(+)}$ with the source for geometric paths (i.e., the usual GTF). The core-scattered wave $\psi_{\text{core}}^{\theta_f}$, arising from an incoming wave at an angle θ_f to the positive z axis, is equated with the source of diffractive semiclassical waves. The closed form expression for $\psi_{\text{core}}^{\theta_f}$ may be given in a partial-wave expansion which, for $m=0$, is [28]

$$\begin{aligned} \psi_{\text{core}}^{\theta_f}(r_0, \theta) = & \left(\frac{2\pi^2}{r_0^3} \right)^{1/4} \sum_{l=0}^{\infty} (-1)^l Y_{l0}^*(\theta_f, 0) Y_{l0}(\theta, 0) \\ & \times e^{i(\sqrt{8r_0} - l\pi - 3\pi/4)} (e^{2i\delta_l} - 1). \end{aligned} \quad (13)$$

A closed form expression for the incoming Coulomb wave can also be derived [25]; for $\theta_f \neq 0$ or π , this is

$$\psi_{\text{Coul}}^{(-)}(r_0, \theta_f) = \frac{\exp\{-i(\sqrt{8r_0} - \pi/2)\}}{\pi\sqrt{8r_0} \sin \theta_f}. \quad (14)$$

For the case where $m=0$, it is also possible for the incoming waves to arise from PO's for which $\theta_f=0$ or π , so that they approach the nucleus along the axis of the fields. In this special case, the closed form expression for $\psi_{\text{Coul}}^{(-)}$ is [28]

$$\psi_{\text{Coul}}^{(-)}(r_0, \theta_f) = \frac{1}{2} \left(\frac{2}{\pi\sqrt{8r_0}} \right) \exp\{-i(\sqrt{8r_0} - \pi/4)\}. \quad (15)$$

We took α to be the fractional amplitude scattered by the core:

$$\alpha_{\text{diff}}(\theta_i, \theta_f) = \psi_{\text{core}}^{\theta_f}(r_0, \theta_i) / \psi_{\text{Coul}}^{(-)}(r_0, \theta_f). \quad (16)$$

For the case of s -wave scattering (and with $\theta_f \neq 0, \pi$), each diffractive contribution in Eq. (10) is

$$\mathcal{G}_k(\theta_i^{(k)}, \theta_f^{(k)}) = B^{1/6} (e^{2i\delta_0} - 1) \left| \frac{2\pi}{m_{12}^{(k)}} \sin \frac{\theta_i^{(k)}}{2} \sin \frac{\theta_f^{(k)}}{2} \right|^{1/2} e^{i\Delta(k)}, \quad (17)$$

where the phase $\Delta_{(k)} = nS_k B^{-1/3} - \mu_{(k)}\pi/2 - \pi/4$, and $m_{12}^{(k)}$ is an element of the 2×2 stability matrix for orbit, k . The contribution of a single-scatter diffractive orbit to the DOS is thus $-(1/\pi)\text{Im}(S_k/i)\mathcal{G}_k(\theta_i^{(k)}, \theta_f^{(k)})$. Although we have not carried out a rigorous derivation including the trace of G_D , we equate our heuristic expression $(S_k/i\hbar)\mathcal{G}_k(\theta_i^{(k)}, \theta_f^{(k)}) = \text{Tr} G_D^k$. The amplitudes in Eq. (17) have been found to yield results for diamagnetic atoms [20] within 1% of the quantal values. Below we test the expressions on parallel atoms and multiple scatters.

For the special case of orbits parallel to the field, the equivalent semiclassical expressions take a different form [20]. Hence, for $\theta_f=0, \pi$,

$$\mathcal{G}_k(\theta_i^{(k)}, \theta_f^{(k)}) = B^{1/3} (e^{2i\delta_0} - 1) \left| \frac{1}{2m_{12}^{(k)}} \right| e^{i\Delta(k)}, \quad (18)$$

where $\Delta_{(k)} = nS_k B^{-1/3} - \mu_{(k)}\pi/2 - \pi/2$. We note that $m_{12}^{(k)}$ is calculated for coordinates normal to the surface of section (i.e., for the semiparabolic coordinate $\mu=0$) rather than normal to the orbit itself.

IV. AMPLITUDE OF FIRST TRAVERSALS OF PERIODIC ORBITS

Diffractive orbits contribute with different phases relative to the geometric and Coulomb terms. For geometric orbits, the phase is given simply by the action plus a topological phase which is related to the Maslov index. The phase Δ for the n th traversal of the k th geometric orbit is

$$\Delta_{nk}^g = nS^k B^{-1/3} - \mu_n^k \pi/2. \quad (19)$$

In general, the topological phase μ_n^k does not scale with traversal number. One-scatter diffractive orbits have an additional phase difference ϕ , accumulated for each scatter. In general, $\phi = -\pi/4 + (\delta_0 + \pi/2)$, with $\phi = -\pi/2 + (\delta_0 + \pi/2)$ for orbits along the z axis, for which $\theta_i^k = \theta_f^k = 0$ or π .

Hence, in the case of first traversals, the Gutzwiller and diffractive pair interferes destructively if $\delta_0 > \pi/4$, leading to genuine ‘‘core shadowing’’ in the sense that the core reduces the amplitude of the oscillation at first traversal. However, if $\delta_0 < \pi/4$, we have constructive interference, and instead we have ‘‘core brightening’’: the amplitude of the nonhydrogenic spectral oscillation is *enhanced* by the core. This explains why quantal amplitudes for contributions from typical primitive PO's of singlet helium (with $\delta_0 = 0.14\pi$) are observed to be enhanced relative to hydrogen, while for lithium they are decreased.

We generated a semiclassical spectrum using contributions of the form given by Eqs. (17) and (18) and products thereof for $\varepsilon_F = -3.0$ and $\varepsilon_B = -0.6$. Our quantal calculations are for $\hbar_{\text{eff}} = B^{1/3} \sim 1/205$. This spectrum was then Fourier transformed. In order to compare the quantal and semiclassical diffractive contributions directly, we adopt the now standard procedure of subtracting the (complex) Fourier transform of the hydrogenic spectrum from that of the nonhydrogenic. This removes the contribution of the geometric orbits, and exposes that of the diffractive trajectories. In addition, all amplitudes (both quantal and semiclassical) were normalized to that of the geometric orbit denoted by R_1 .

In the pure magnetic field case, R_1 is the well-known ‘‘quasi-Landau’’ PO, which corresponds to a straight line trajectory perpendicular to the magnetic field. In that case R_1 runs along a symmetry boundary and its Gutzwiller contribution has an additional phase. In the parallel field case, R_1 still lies on a straight line orbit, but is no longer perpendicular to the fields [see orbit (a) in Fig. 2]. Its Gutzwiller amplitude is given by the usual form and the contribution to $\text{Tr} G_g$ is

$$\text{Tr} G_g^{R_1} = -i \frac{S_{R_1}}{|m_{11} + m_{22} - 2|^{1/2}} e^{i\Delta_{R_1}^g}. \quad (20)$$

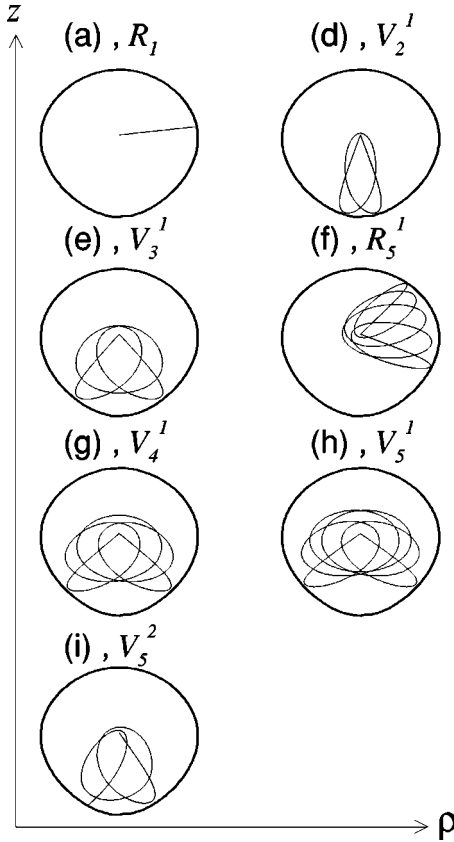


FIG. 2. Classical periodic orbits of the hydrogen atom in parallel static electric and magnetic fields with $\varepsilon_F = -3.0$ and $\varepsilon_B = -0.6$. The trajectories are plotted in the ρz plane. The heavy line denotes the classical turning surface. Only those orbits that contribute to the semiclassical spectra for scaled action $S/(2\pi) \leq 5$ are shown. Labels (a)–(i) correspond to the scheme used to identify the peaks in Figs. 4 and 5. Each orbit is also identified by its corresponding diamagnetic orbit using the naming convention introduced in Ref. [2]. Not shown are the (b) ‘‘uphill’’ and (c) ‘‘downhill’’ straight-line orbits that run along the $\pm z$ axis, and were denoted V_1^+ and V_1^- , respectively, in Ref. [32].

The corresponding contribution to $\text{Tr } G_D$ from the one-scatter diffractive orbit is

$$\text{Tr } G_D^{R_1} = -i S_{R_1} B^{1/6} \left| \frac{8\pi}{m_{12}^{(R_1)}} \right|^{1/2} \sin \delta_0 \sin \frac{\theta_i}{2} e^{i(\Delta_{R_1}^g + \pi/4 + \delta_0)}. \quad (21)$$

In parallel field terminology the perturbed R_1 PO is labeled PO a . In order to stress that this is not a diamagnetic atom, we label the PO’s as a, b, c , etc., in our Fourier transforms. The main PO’s are plotted in Fig. 2, where both the parallel field label and that for the pure diamagnetic PO (into which the PO evolves as the electric field is switched off) are shown. For the R_1 (a) PO, the classical parameters are $S_{R_1}/(2\pi) = 0.8258$, $m_{11} = m_{22} = 0.7135$, $m_{12} = -1.282$, and $\theta_i = \theta_f = 0.449\pi$. With these parameters it is easy to show with a pocket calculator that, for an atom with $\delta_0 = 0.5\pi$, the ratio of the amplitude $|\text{Tr } G_D^{R_1}|$ from Eq. (21) to the normalization amplitude ($|\text{Tr } G_g^{R_1}| = 1.3211 S_{R_1}$), is $|\text{Tr } G_D^{R_1}|/|\text{Tr } G_g^{R_1}| = 0.152$. This value is seen below to correspond ac-

curately to the (normalized) quantum peak height for the single diffraction PO. This peak is labeled $a+$ in our Fourier transforms [see Fig. 5(a)]. We now consider degeneracies and multiplicities of the different types of diffractive contributions.

V. MULTIPLICITY OF DIFFRACTIVE ORBITS

Multiple-scatter contributions can, in the atomic case, include different combinations of geometric and diffractive orbits which all have the same actions (core shadowing). We note that, although core shadowing does not affect primitive contributions in closed orbit theory, it affects both the primitive PO’s and their repetitions in diffractive PO theory [20]. In order to describe core shadowing, it is vital that the contributions from the different combinations and, in particular their phases, are combined correctly.

For example, below we demonstrate in detail the construction of diffractive contributions interfering with the third traversal of one specific isolated PO, namely, R_1 . In the notation of Ref. [2], its second and third traversals are denoted R_2 and R_3 , respectively.

The contribution to the DOS has a phase equal to $3S_{R_1} B^{-1/3} + \Omega$. The additional phase Ω varies depending on the type of contribution: (i) for the purely geometric contribution, $\Omega = \mu_{R_3} \pi/2$; (ii) for one-scatter contributions, $\Omega = \mu_{R_3} \pi/2 + \phi$; (iii) for two-scatter contributions, $\Omega = \mu_{R_1} \pi/2 + \mu_{R_2} \pi/2 + 2\phi$; and (iv) for three-scatter terms, $\Omega = 3\mu_{R_1} \pi/2 + 3\phi$. In this example, with $\delta_0 = 0.5\pi$, we have $\phi = 3\pi/4$.

The one- and two-scatter orbits are in effect combinations of geometric and diffractive ‘‘legs’’ in the same trajectory, since each encounter with the core can result in either geometric or diffractive scattering. The three-scatter contribution is a combination of three diffractive orbits. We stress that these hybrid PO’s, combining diffractive and geometric core scatters, are a unique feature of the atomic systems (due to combined Coulomb plus short-range scattering). Generic diffractive billiards have pure geometric and pure diffractive orbits, which are unrelated, and in general have different actions.

We have found that the amplitude of a single diffractive orbit as given in Eq. (17) is weighted by a degeneracy g_k . For a primitive symmetric orbit ($\theta_f = \theta_i$), $g_k = 1$. For a primitive asymmetric orbit ($\theta_f \neq \theta_i$), $g_k = 2$. We attribute this weighting to the fact that, for each incoming Coulomb wave, the diffracted wave provides amplitude in one or two possible outgoing angles, respectively.

Another key parameter is the multiplicity or degeneracy of multiple traversals. The one-scatter orbits have a multiplicity equal to the repetition number of the orbit. Hence for the one-scatter contribution to the n th traversal, $g_{nk} = n g_k$. This is due to the number of different permutations of geometric and diffractive scatters.

For example, the one-scatter contribution to R_3 has three possible permutations of geometric or diffractive encounters with the core. One of these can be represented as $R_1 + R_1 X R_1 X$, where $R_1 +$ indicates a traversal of the PO, $R_1 X$ indicates a traversal followed by diffraction, and $R_1 X$ indicates a traversal followed by a Coulomb scatter. The other two possible permu-

tations are $R_1XR_1+R_1X$ and $R_1XR_1XR_1+$. Hence, from Eq. (17), the contribution to the trace from each one-scatter diffractive orbit is $-iS_{R_1}\mathcal{G}_{R_3}$ where,

$$\mathcal{G}_{R_3} = B^{1/6} \left| \frac{8\pi}{m_{12}^{(R_3)}} \right|^{1/2} \sin \frac{\theta_i}{2} e^{i(\Delta_{R_3}^g + 3\pi/4)}. \quad (22)$$

In this case, $g=1$ and $\Delta_{R_3} = 3S_{R_1} + \mu_{R_3}\pi/2$. From the monodromy matrix elements given above for R_1 , we can work out that $m_{12}^{(R_3)} = -1.329$. This contribution has a multiplicity of 3. Hence from Eq. (22) we can evaluate the total amplitude (normalized by the geometric amplitude of R_1), which is $3|S_{R_1}\mathcal{G}_{R_3}|/|\text{Tr}G_D^{R_1}| = 0.447$. The quantal value is 0.4. For improved agreement, higher order diffractive scatters must be included. We note, however, that the one-scatter diffractive contribution for R_3 is already almost 50% of the geometric amplitude of the first traversal.

In general, the number of s -scatter diffractive trajectories contributing to the n th traversal of a PO is simply the number of combinations, and is given by the usual binomial coefficient: $N(n,s) = n! / [(n-s)!s!]$. An important consequence is that, while in the GTF the n th traversal of the k th geometric PO is weighted by the *primitive* period T_k (in the unscaled case) or action S_k (in the scaled case), the corresponding one-scatter component is weighted by the *total* period nS_k . Hence for high enough repetition numbers $n \sim \hbar^{-1/2}$ even the one-scatter diffractive contribution becomes of the same order as the geometric PO contribution.

For the two-scatter diffractive case, there are $n(n-1)/2$ possible trajectories. Hence this component will be significant for $n^2 \sim \hbar^{-1}$. We conclude that multiple traversals of PO's will also have significant two-scatter components for a sufficiently high number of traversals. In the case of the R_3 orbit, the two-scatter orbits have a multiplicity $N(3,2) = 3$. Their total contribution to $\text{Tr}G_D$ is equal to

$$-i3g^2S_{R_1}\mathcal{G}_{R_1}\mathcal{G}_{R_2}. \quad (23)$$

Here $g=1$. Since $m_{12}^{(R_2)} = -1.8298$, we can evaluate $3|S_{R_1}\mathcal{G}_{R_1}\mathcal{G}_{R_2}|/|\text{Tr}G_D^{R_1}| = 0.0764$.

This contribution is dephased by $3\pi/4$ relative to the one-scatter diffractive contribution of 0.447. However adding these values with the correct dephasing is easily shown to yield a value very close to the quantal peak ~ 0.4 shown in Fig. 3. For this particular example, Maslov indices scale with the traversal, i.e., $\mu_{R_1} + \mu_{R_2} = \mu_{R_3}$. But this is not generally the case. Although the total number of two-scatter core-shadowing corrections is always $N(n,2)$, for detailed studies of higher traversals it is not possible to simply weight one expression such as Eq. (23) by a multiplicity, $N(n,2)$, since in general there will be different combinations of two orbits. For example, if we were considering the two-scatter correction to R_6 we would have $N(6,2) = 15$ contributions. However, six of these would involve $\mathcal{G}_{R_2}\mathcal{G}_{R_4}$ terms, another six would involve $\mathcal{G}_{R_1}\mathcal{G}_{R_5}$ terms, and three would involve $\mathcal{G}_{R_3}\mathcal{G}_{R_3}$ terms. These three groups have different phases, so care must be taken when combining them.

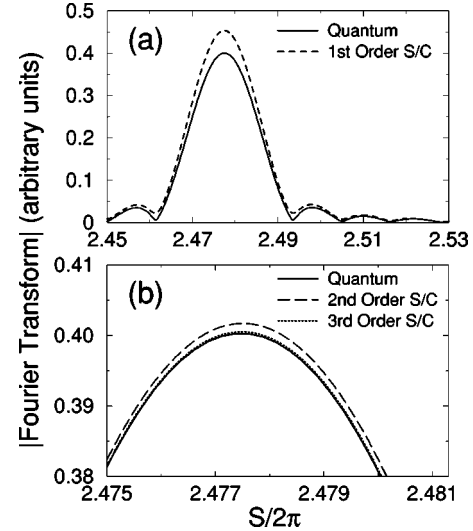


FIG. 3. Contributions from diffractive PO's at the action of PO $3a$, the third repetition of the PO a . PO a is the parallel field PO which evolves (in the limit of zero electric field) into the diamagnetic PO R_1 , responsible for quasi-Landau modulations observed in atomic photoabsorption spectra. (a) Comparison between quantum (full line) and semiclassical (dashed line) results using only one-scatter diffractive trajectories. The results show that at this value of $\hbar_{\text{eff}} \approx 1/205$, including contributions from one-scatter trajectories reproduces the quantal result to within 10–15%. (b) Comparison with quantal amplitudes (full line) including up to two- (dashed line) and three-scatter (dotted line) trajectories. Including the two-scatter trajectories already brings the agreement with the quantal results to well within 1%. The graphs had to be magnified substantially to show any difference between the semiclassical result including three-scatter orbits and the quantal amplitude.

The final and smaller contribution to R_3 , the three-scatter term, has a multiplicity $N(3,3) = 1$. Hence its contribution is equal to

$$-i \frac{S_{R_1}}{i\pi} \mathcal{G}_{R_1}\mathcal{G}_{R_1}\mathcal{G}_{R_1}. \quad (24)$$

We have tested the counting algorithm by including successively the contributions from one-, two- and three-scattering trajectories at a scaled action corresponding to R_3 ; the results for a nonhydrogenic atom with a single quantum defect $\delta_0 = 0.5\pi$ in the $l=0$ channel are shown in Fig. 3.

In Fig. 3(a) we compare the resulting quantum amplitude with the first-order semiclassical result obtained using Eq. (22). At this value of $\hbar_{\text{eff}} \approx 1/205$, single-scattering trajectories (dashed line) reproduce the quantum amplitude (full line) to within 10–15%. Figure 3(b) shows the results of including second- and third-order terms, for which the contributions to $\text{Tr}G_D$ are given by Eqs. (23) and (24), respectively, in the semiclassical calculation. Including the second-order terms (dashed line) already brings the agreement with the quantal results (full line) to within 1%. When third-order terms are included, the semiclassical (dotted line) and quantal amplitudes agree almost exactly. The excellent agreement for the third-order terms seen in Fig. 3(b) strongly supports our counting algorithm.

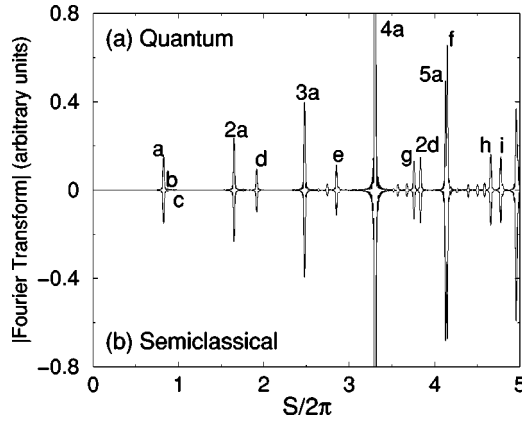


FIG. 4. Comparison between quantum and semiclassical results for all periodic orbits up to the scaled action $S/2\pi = 5$, including all orders of scattering. The agreement is excellent except where bifurcation effects are significant. Labeled peaks correspond to the classical periodic orbits shown in Fig. 2.

However, two-scatter combination orbits will proliferate sufficiently rapidly to ensure that their contribution is not semiclassically vanishing relative to the primitive geometric PO's. For an integrable system, the total number of PO's grows polynomially with the period, as T^2 in our two-dimensional system and as S^2 in the scaled case. The total two-scatter combination orbits can easily be shown to proliferate as T^4 (or S^4). Hence their contribution, relative to that of the geometric PO's, for sufficiently long periods or actions, does not vanish.

The rules for obtaining multiplicities of two-scatter contributions of different orbits are analogous to those used above for the multiple traversals [34]. Below, we apply these rules for accumulating phases and multiplicities in our semiclassical calculations for the range $0 \leq S/(2\pi) \leq 5$ and compare them with quantal calculations.

VI. RESULTS

The main result of this paper is shown in Fig. 4, where we compare quantal and semiclassical results for the total diffractive component up to action $S/2\pi = 5$. As in Fig. 3, we coherently subtract the Fourier transformed quantal spectra for $\delta_0 = 0.5\pi$ from the hydrogenic result, so we compare only the diffractive quantal and semiclassical result. The overall agreement is excellent. Indeed, on the scale of the figure, there are barely any discernible differences between the quantum and semiclassical diffractive contributions. The labeled peaks indicate diffractive contributions at scaled actions corresponding to the short classical periodic orbits of the hydrogen atom in parallel fields; the shapes of these orbits were shown in Fig. 2.

In Fig. 5 we magnify selected regions of Fig. 4 in order to further demonstrate the agreement. Figure 5(a) shows a magnification of the spectra in the region $0.75 \leq S/(2\pi) \leq 1.0$. In this region, we see three peaks corresponding to the diffractive contributions, $a+$, $b+$, and $c+$. For each of the peaks, the semiclassical result in the lower panel agrees almost perfectly with the exact quantum result in the upper panel. Here we see that the core-shadowing terms give rise to large contributions at scaled actions of the primitive periodic orbits.

This is in contrast to the closed orbit result for nonhydrogenic photoabsorption spectra, where it was shown that the core-shadowing terms only alter the phase of the primitive orbit contributions while leaving their amplitudes unchanged. The peaks labeled $b+$, at $S/(2\pi) \approx 0.88$, and $c+$, at $S/(2\pi) \approx 0.96$, are the core-shadowed contributions to the ‘‘uphill’’ (V_1^+) and ‘‘downhill’’ (V_1^-) orbits, respectively. As can be seen by comparing Eqs. (17) and (18), the diffractive contributions to both of these orbits are $O(\hbar^{1/2})$, smaller than those for orbits with $\theta_i \neq 0$ or π . Hence peaks $b+$ and $c+$ are considerably smaller than that of the R_1 orbit at $a+$.

In Fig. 5(b) we show the region of scaled action close to the contributions from the second repetitions of the orbits a , b , and c [$1.5 \leq S/(2\pi) \leq 2.0$]. Again, the agreement between quantal and semiclassical calculations is excellent. Here the largest contribution is to the second repetition of the R_1 orbit at $S/(2\pi) \approx 1.65$. This contribution consists of two terms: $2a+$ and $a+a+$ of $O(\hbar^{1/2})$ and $O(\hbar)$, respectively. The peak at the second repetition of the downhill orbit at $S/(2\pi) \approx 1.92$ is larger than might be expected given that the terms $2c+$ and $c+c+$ are $O(\hbar)$ and $O(\hbar^2)$, respectively. However, here there is also an $O(\hbar^{1/2})$ contribution from the V_2^1 orbit (labeled $d+$). The inset shows a further magnification of the region $1.7 \leq S/(2\pi) \leq 1.84$, where two further small peaks can be seen: one at the second repetition of the uphill orbit at $S/(2\pi) \approx 1.76$, and a second, purely core-scattered peak, arising from a combination of contributions from the R_1 ($a+$) and downhill ($c+$) orbits.

Figure 5(c) magnifies the region $3.2 \leq S/(2\pi) \leq 3.9$. Overall, the quantum-semiclassical agreement is very good. A close inspection, however, reveals two small discrepancies. For the peak at the fourth repetition of R_1 [$S/(2\pi) \approx 3.3$] the semiclassical result overestimates the quantal result by about 50%. This is due to the m_{12} term that appears in the amplitude being close to zero for the $4a+$ contribution. This leads to a singularity in the semiclassical amplitude of this term. Such a phenomenon occurs when the classical orbit undergoes a bifurcation, in which case its winding number is nearly rational. Here the winding number for the R_1 or a PO is close to $1/8$.

It is interesting to note that a given bifurcation can manifest itself at different actions in the diffractive and geometric contributions. For the geometric contribution, the amplitude is proportional to $1/\sqrt{\text{Tr} M - 2}$, and will be unphysically large for the eighth repetition of the orbit when the winding number of the primitive orbit is $1/8$. For the diffractive contribution, on the other hand, the amplitude is proportional to $1/\sqrt{m_{12}}$, and will be divergent for the fourth repetition of the orbit. This particular large diffractive peak at the action of $4a$ is due to an asymmetric closed orbit, which appears at half the period of $8a$.

A similar small discrepancy in the diffractive amplitudes is also seen for the peak at $S/(2\pi) \approx 3.57$, which has been further magnified in the right-hand inset. Again, this small difference between quantal and semiclassical results can be attributed to a bifurcation in the underlying classical dynamics.

Finally, a magnification of the region $4.05 \leq S/(2\pi) \leq 4.2$ is shown in Fig. 5(d). Again, the unphysically large

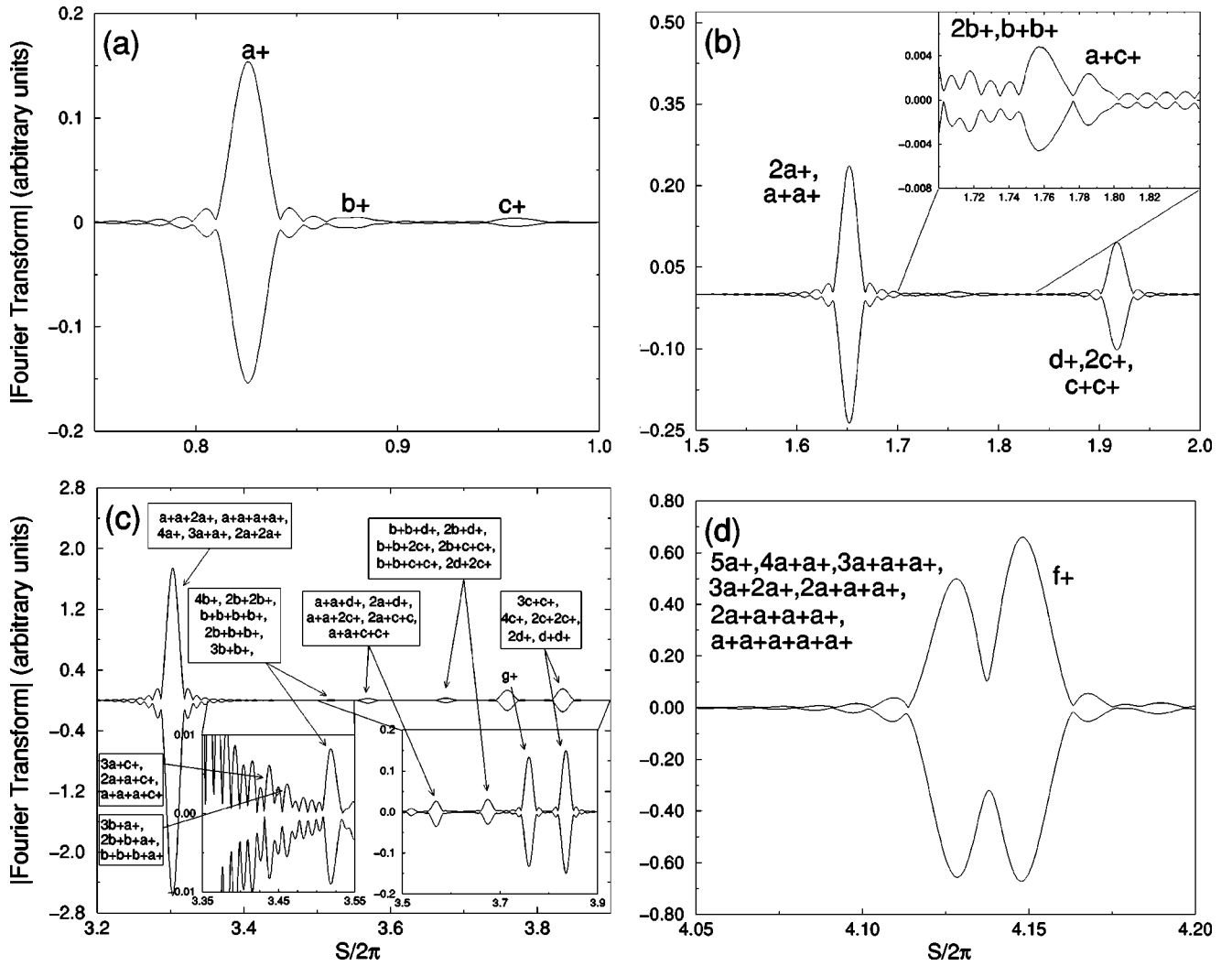


FIG. 5. Magnification of parts of the spectrum presented in Fig. 4. Shown are the regions (a) $0.75 \leq S/(2\pi) \leq 1.0$; (b) $1.5 \leq S/(2\pi) \leq 2.0$; (c) $3.2 \leq S/(2\pi) \leq 3.9$, and (d) $4.05 \leq S/(2\pi) \leq 4.2$. The figure shows that diffractive orbit contributions are described with extreme accuracy. For completeness we indicate and include all possible scattering combinations contributing to each peak although, clearly, the contribution of fourth and higher scattering combinations, for these low actions, is extremely small.

value of the diffractive amplitude for the $4a+$ contribution leads to the semiclassical result overestimating the quantum, this time by about 10%, for the peak at $S/(2\pi) \approx 4.125$. However, again the agreement between the quantal and semiclassical spectra is remarkable, especially bearing in mind that the peak at $S/(2\pi) \approx 4.125$ is made up of no fewer than seven different contributions; this in fact represents the most challenging situation we have considered to date.

VII. CONCLUSIONS

We have shown that the spectra of atoms in parallel fields provide an interesting illustration of the effects of diffractive PO's in a real system. Features like the core brightening and core shadowing as well as the hybrid diffractive and geometric scatter PO's are unique features of the atomic core scattering, and are needed to describe the quantum results accurately.

Until quite recently, it seemed apparent that diffractive orbits represented \hbar -dependent corrections to periodic orbit effects which vanished in the semiclassical limit. Now it

seems clear that, for sufficiently long time scales, such diffractive effects can persist in the $\hbar \rightarrow 0$ limit. Hence understanding how the proliferation of diffractive orbits sufficiently outpaces, at any order, the proliferation of geometric trajectories to maintain their contribution, as $\hbar \rightarrow 0$, is an interesting and topical question.

In this study we focused on the near-integrable atomic regime. The combination of Coulomb and short-range scattering introduces interference effects that to our knowledge have not been seen in typical systems such as billiards with short-range scattering.

Previously, we presented a model which gave diffractive corrections for a diamagnetic atom. However, the proper way to count contributions from higher-order scatterings, multiple repetitions, and combinations thereof remained unclear. We have extended the model to account for harmonics (important in the stable regime), and have tested this on atoms in parallel fields. The physics is not drastically different from the diamagnetic case, but the different symmetry and the fact that the important quasi-Landau orbit (R_1 or a and its repetitions) no longer lies on the symmetry boundary provides a

strong test of the general validity of the model. We have shown that the model yields amplitudes and phases with great accuracy. The agreement is generally well within a few percent, except where bifurcation effects (neglected in the semiclassics) become important.

ACKNOWLEDGMENTS

We thank Paul Walker and Peter Braun for useful discussions. This work was supported in part by the EPSRC and also by the British Council through the Alliance Programme.

-
- [1] *Irregular Atomic Systems and Quantum Chaos*, edited by J.-C. Gay (Gordon and Breach, London, 1992).
- [2] A. Holle, J. Main, G. Wiebusch, H. Rottke, and K. H. Welge, *Phys. Rev. Lett.* **61**, 161 (1988).
- [3] H. Hasegawa, M. Robnik, and G. Wunner, *Suppl. Prog. Theor. Phys.* **98**, 198 (1989).
- [4] H. Friedrich and D. Wintgen, *Phys. Rep.* **183**, 37 (1989).
- [5] T. S. Monteiro and G. Wunner, *Phys. Rev. Lett.* **65**, 1100 (1990).
- [6] D. Delande, K. T. Taylor, M. H. Halley, T. van der Veldt, W. Vassen, and W. Hogervorst, *J. Phys. B* **27**, 2771 (1994).
- [7] D. Wintgen, *Phys. Rev. Lett.* **58**, 1589 (1987).
- [8] M. C. Gutzwiller, *Chaos in Classical and Quantum Mechanics* (Springer-Verlag, New York, 1990).
- [9] M. Courtney, H. Jiao, N. Spellmeyer, and D. Kleppner, *Phys. Rev. Lett.* **73**, 1340 (1994).
- [10] T. Jonckheree, B. Gremaud, and D. Delande, *Phys. Rev. Lett.* **81**, 2442 (1998).
- [11] K. Karremans, A. Kips, W. Vassen, and W. Hogervorst, *Phys. Rev. A* **60**, R2649 (1999).
- [12] D. Braun, G. Montambaux, and M. Pascaud, *Phys. Rev. Lett.* **81**, 1062 (1998).
- [13] B. L. Altshuler, Y. Gefen, A. Kamenev, and L. Levitov, *Phys. Rev. Lett.* **78**, 2803 (1997).
- [14] M. Pascaud and G. Montambaux, *Ann. Phys. (Leipzig)* **7**, 406 (1998).
- [15] E. B. Bogomolny, U. Gerland, and C. Schmidt, *Phys. Rev. E* **59**, R1315 (1998).
- [16] W. Jans, T. S. Monteiro, W. Schweizer, and P. A. Dando, *J. Phys. A* **26**, 3187 (1993).
- [17] P. A. Dando, T. S. Monteiro, W. Jans, and W. Schweizer, *Suppl. Prog. Theor. Phys.* **116**, 403 (1994).
- [18] B. Hüpfer, J. Main, and G. Wunner, *Phys. Rev. Lett.* **74**, 2650 (1995); *Phys. Rev. A* **53**, 744 (1996).
- [19] P. A. Dando, T. S. Monteiro, D. Delande, and K. T. Taylor, *Phys. Rev. Lett.* **74**, 1099 (1995); *Phys. Rev. A* **54**, 127 (1996).
- [20] P. A. Dando, T. S. Monteiro, and S. M. Owen, *Phys. Rev. Lett.* **80**, 2797 (1998).
- [21] P. N. Walker and T. S. Monteiro, e-print, chao-dyn/9911008.
- [22] M. Sieber, *J. Phys. A* **32**, 7679 (1999).
- [23] G. Vattay, A. Wirzba, and P. E. Rosenqvist, *Phys. Rev. Lett.* **73**, 2304 (1994); H. Primack, H. Schanz, U. Smilansky, and I. Ussishkin, *ibid.* **76**, 1615 (1996).
- [24] H. Bruus and N. D. Whelan, *Nonlinearity* **9**, 1023 (1996).
- [25] M. L. Du and J. B. Delos, *Phys. Rev. A* **38**, 1896 (1988); **38**, 1913 (1988).
- [26] E. B. Bogomolny, *Zh. Éksp. Teor. Fiz.* **96**, 487 (1989) [*Sov. Phys. JETP* **69**, 275 (1989)].
- [27] G. Alber, *Z. Phys. D: At., Mol. Clusters* **14**, 307 (1989).
- [28] J. Gao, J. B. Delos, and M. Baruch, *Phys. Rev. A* **46**, 1449 (1992); J. Gao and J. B. Delos, *ibid.* **46**, 1455 (1992).
- [29] C. W. Clark and K. T. Taylor, *J. Phys. B* **15**, 1175 (1982).
- [30] M. V. Berry and M. Tabor, *Proc. R. Soc. London, Ser. A* **349**, 101 (1976); *J. Phys. A* **10**, 371 (1977).
- [31] S. Tomsovic, M. Grinberg, and D. Ullmo, *Phys. Rev. Lett.* **75**, 4346 (1995).
- [32] M. Courtney, *Phys. Rev. A* **51**, 4558 (1995).
- [33] H. Friedrich, *Theoretical Atomic Physics* (Springer-Verlag, New York, 1990).
- [34] S. M. Owen., Ph.D. thesis, University College London, 2000 (unpublished).